Boosting Brain Signal Variability Underlies Liberal Shifts in Decision Bias

Niels A. Kloosterman[1,2*], Julian Q. Kosciessa[1,2], Ulman Lindenberger[1,2], Johannes Jacobus Fahrenfort[3], Douglas D. Garrett[1,2]

[1]Max Planck UCL Centre for Computational Psychiatry and Ageing Research and [2]Center for Lifespan Psychology, Max Planck Institute for Human Development, Lentzeallee 94, 14195 Berlin, Germany

[3]Department of Experimental and Applied Psychology, Vrije Universiteit, van der Boechorststraat 1, 1081 BT Amsterdam, The Netherlands

[4]Department of Psychology, University of Amsterdam, The Netherlands;

*****Correspondence: Niels Kloosterman

Email: kloosterman@mpib-berlin.mpg.de

Author ORCIDs
Niels A Kloosterman http://orcid.org/0000-0002-1134-7996
Julian Kosciessa https://orcid.org/0000-0002-4553-2794
Ulman Lindenberger https://orcid.org/0000-0001-8428-6453
Johannes Jacobus Fahrenfort http://orcid.org/0000-0002-9025-3436
Douglas D Garrett https://orcid.org/0000-0002-0629-7672

Classification
Biological Sciences / Neuroscience

Keywords
Brain signal variability, decision bias, perceptual decision making, signal detection theory

Author Contributions
Niels Kloosterman, Conceptualization, Data curation, Software, Formal analysis, Investigation, Visualization, Methodology, Writing—original draft, Project administration, Writing—review and editing; Julian Kosciessa, Software, Formal analysis, Writing—review and editing; Ulman Lindenberger, Resources, Funding acquisition, Writing—review and editing; Johannes Jacobus Fahrenfort, Conceptualization, Data curation, Software, Formal analysis, Supervision, Visualization, Methodology, Writing—original draft, Project administration, Writing—review and editing; Douglas Garrett, Conceptualization, Resources, Formal analysis, Supervision, Funding acquisition, Investigation, Methodology, Writing—review and editing.

This PDF file includes:
Main Text
Figures 1 to 6

Abstract

Strategically adopting decision biases allows organisms to tailor their choices to environmental demands. For example, a liberal response strategy pays off when target detection is crucial, whereas a conservative strategy is optimal for avoiding false alarms. Implementing strategic bias shifts is presumed to rely on prefrontal cortex, but the temporal signature of such biases remains elusive. We hypothesized that strategic liberal bias shifts during a continuous target detection task arise through a more unconstrained neural regime (higher entropy) suited to the detection of unpredictable events. Human participants performed a visual target detection task reporting faint target stimuli within a stream of non-targets via button press, while we measured their electroencephalogram (EEG). Subjects were instructed in separate conditions to maximize the number of detected targets ('liberal' condition) and to minimize false detections ('conservative' condition) by penalizing either missed targets or false alarms. To measure neural variability, we developed a novel algorithm based on multi-scale entropy (MSE) that directly quantifies the temporal irregularity of the EEG signal in longer and shorter timescales. Upregulation of entropy in frontal brain regions indeed strongly characterized the degree to which individuals shifted from a conservative to a liberal bias, both across subjects and within single participants. Overall EEG signal variation and oscillatory (spectral) dynamics could not account for this relationship. Our results suggest that modulation of neural variability in frontal regions is instrumental for permitting an organism to tailor its decision bias to environmental demands.

Significance Statement

The ability to bias choices depending on the task context allows organisms to adapt to their environment. A liberal bias, for example, suits a situation when it is crucial to detect all events that might unpredictably occur, whereas a more conservative attitude pays off when avoiding errors is key. How the brain maintains such biased states over time remains unknown. We hypothesized that strategic liberal bias shifts arise through more unconstrained, irregular neural activity (higher entropy) suited to an unpredictable environment. Enhanced entropy in frontal regions indeed strongly reflected how much individuals shifted their bias to become more liberal. Modulation of neural variability through prefrontal cortex thus appears instrumental for tailoring decision biases to environmental demands.

Main text

Introduction

We often reach decisions not only by objectively weighing different alternatives, but also by allowing subjective decision biases to influence our choices. Ideally, such biases should be under internal control, allowing us to flexibly adapt to changes in task context while performing a challenging task. Specifically, contexts which prioritize target detection benefit from a liberal response strategy, whereas a conservative strategy should be used at times when it is important to avoid errors of commission (e.g., false alarms). Strategic shifts in decision bias are presumed to rely on a neural process in prefrontal cortex (1). However, despite growing interest (2–4), the spatio-temporal neural signature of such within-person bias shifts is unknown. As such, how strategic decision biases are neuronally implemented and retained during a specific task context remain open questions.

One candidate neural signature of decision bias shifts that has not been considered thus far is moment-to-moment variability of brain activity. Temporal neural variability is a prominent feature in all types of neural recordings (single-cell, local field potentials, EEG/MEG, fMRI) and traditionally has been considered 'noise' that corrupts neural computations. However, increasing evidence suggests that temporal variability can instead prove optimal for neural systems, allowing individuals to perform better, respond faster, and adapt quicker to their environment (5–7). Here, we perform a crucial test of the utility of moment-to-moment neural variability in the context of adaptive human decision making. We hypothesized that within-person upregulation of neural variability would implement a strategic, liberal bias shift that 'opens up' the decision-making process more widely to target input from the environment (8, 9). Specifically, we reasoned that increased neural variability might underlie a state of higher receptiveness to, and preparedness for, events of interest that occur at unpredictable moments in time, thus allowing the decision maker to adopt a more liberal bias towards deciding that such an event has indeed occurred.

We addressed this hypothesis using data from humans performing a challenging, continuous target detection task under two different decision bias manipulations, while non-invasively recording their electroencephalogram (EEG) (10). Sixteen participants (three experimental sessions each, mean of 1733 trials/participant) were asked to detect orientation-defined squares within a continuous stream of line textures of various orientations and report targets via a button press (Figure 1A). In alternating nine-minute blocks of trials, we actively biased participants' perceptual decisions by instructing them either to report as many targets as possible (liberal condition), or to only report high-certainty targets (conservative condition). We played auditory feedback after errors and imposed monetary penalties to enforce instructions. We quantified the decision biases in both conditions with a criterion measure from signal detection theory (SDT) (11), and developed a novel, modified multi-scale entropy (mMSE) algorithm (12) to measure temporal variability in the time-domain EEG signal. We tested our hypothesis by change-change correlating the liberal–conservative shifts in decision bias and mMSE, both across and within participants. As entropy measures in neuroimaging are often confounded by fluctuations in overall signal variation and spectral power (13), we investigated the unique contribution of temporal neural variability to the bias shifts by explicitly controlling for the standard deviation of the EEG signal as well as power in canonical frequency bands (delta up to gamma). Finally, rather than a rise

in neural variability, previous work has linked a transient variability reduction (referred to as 'quenching') to improved cognitive ability (14–16). We examined whether quenching also occurs in entropy and to what extent it is related to behavior in our task.

[INSERT FIGURE 1 AROUND HERE]

Results

Participants differentially adopted the intended decision biases in the respective conditions, as quantified with SDT criterion. Subjects assumed a lower criterion (more liberal bias) when target detection was emphasized (c = –0.13, standard deviation (SD) 0.4) and adopted a higher criterion (more conservative bias) when instructed to avoid false alarms (c = 0.73, SD 0.36; liberal vs. conservative, p = 0.001, two-sided permutation test, 10,000 permutations)(Figure 1B). Participants varied substantially not only in the average criterion they used across the two conditions (range of c = –0.24 to 0.89), but also in the size of the criterion shift between conditions (range of Δc = –1.54 to –0.23). Highlighting the extent of individual differences, participant's biases in the two conditions were only weakly correlated (Spearman's rho = 0.24, p = 0.36), as can be seen from the subjects' large variation in criterion intercept and slope between the two conditions in Figure 1C. Moreover, the bias shift also fluctuated within participants to some extent over the course of the experiment, as indicated by variation in criterion differences between successive, nine-minute liberal and conservative blocks (participant-average SD 0.37, Figure 1D). Taken together, we observed considerable variability in strategic decision bias shifts both at the group level and within single individuals.

We exploited the between- and within-participant variations in liberal–conservative criterion differences to test our hypothesis that a boost in brain signal variability underlies a liberal bias shift. To this end, we developed a novel algorithm based on multi-scale entropy (MSE) that directly quantifies the temporal irregularity of the EEG signal at longer and shorter timescales (12). In general, patterns of fluctuations in brain activity that tend to repeat over time, such as neural oscillations, are assigned lower entropy, whereas more irregular, non-repeating patterns yield higher entropy (13). We developed time-resolved, modified MSE (mMSE), a measure that allows tracking of entropy over the course of the trial by calculating entropy across discontinuous, aggregated segments taken across trials via a sliding window approach (Figure 2)(17).

[INSERT FIGURE 2 AROUND HERE]

We tested for a relationship between shifts in decision bias and neural variability between the conservative and liberal conditions by correlating joint modulations of mMSE and criterion across participants (averaged over the three sessions), for all electrodes, time points, and timescales. Strikingly, we found a negative cluster of correlations in mid- and left-frontal electrodes (after cluster-correction for multiple comparisons (18), cluster p = 0.022) indicating that participants who showed a larger bias shift from the conservative to the liberal

condition also exhibited a larger boost in frontal entropy (Figure 3A). The cluster ranged across timescales from ~20-164 ms, with most of the cluster located after trial initialization (solid vertical line in Figure 3A). To illustrate this correlation, we averaged liberal–conservative mMSE within the significant cluster and plotted the across-participant change-change correlation (rho = –0.90) with criterion (Figure 3B).

[INSERT FIGURE 3 AROUND HERE]

We next employed several approaches to strengthen evidence for the observed link between shifts in neural variability and decision bias. First, we asked whether mMSE and bias were also linked within participants across the nine liberal–conservative block pairs (see Figure 1A, bottom and 1D). Critically, we found a negative repeated measures correlation between within-participant shifts in criterion and mMSE (19)(r_{rm} = –0.19, p = 0.039, Figure 3C), providing convergent within-person evidence for a link between shifts in decision bias and neural variability. Second, we tested the reliability of the change-change correlation across participants by performing the analysis separately for odd and even trials. We found significant correlations in both arbitrary data halves (odd, rho = –0.61, p = 0.013; even, rho = –0.64, p = 0.009, see Figure S2), indicating that the observed relationship is indeed reliable.

Third, we investigated whether the correlation could be explained by various potentially confounding factors. Specifically, entropy estimates can be affected by the time-domain signal SD through the pattern similarity (r) parameter (see Figure 2), even when this parameter is recomputed after each coarsegraining step (13, 20). This is because the r parameter is defined as a proportion of the signal SD, which determines how lenient the algorithm is towards labeling a pattern as a repeat. Due to this dependence of the r parameter on signal SD, higher SD can yield lower indicated entropy and vice versa, possibly resulting in negative correlations between the two metrics. In addition, electrophysiological (e.g., EEG) data is often quantified in terms of oscillatory spectral power in canonical delta (1-2 Hz), theta (3-7 Hz), alpha (8-12 Hz), beta (13-30 Hz) and gamma (60-100 Hz) bands, which might be related to entropy. Therefore, we tested whether the Δbias-Δentropy correlation could be explained by broadband signal SD and oscillatory spectral power. To make the computation of spectral power and entropy as similar as possible, we used the same 0.5 s sliding window and 50 ms step size for spectral analysis (1 s window to allow delta power estimation, see methods), and selected spectral power within the same electrodes and time points in which the mMSE effect was indicated. Strikingly, we found that the Δbias-Δentropy correlation remained strong and significant both when controlling for signal SD (partial rho = –0.82, p < 0.0001), and when controlling for all major power bands simultaneously (delta, theta, alpha, beta, gamma; partial rho = –0.68, p = 0.02) (Figure S3). Moreover, we found no significant clusters when correlating the bias shift with liberal–conservative spectral power modulation normalized with respect to the pre-stimulus baseline, indicating that power modulation also does not track bias shifts (Figure S5). Interestingly, explicitly controlling for overall signal variation (SD) in each time-scale bin in each electrode via partial correlation narrowed the cluster of significant correlations down to timescales from 20-80 ms (Figure 4A), suggesting that the slower timescales implicated in the mMSE correlation in Figure 3A are primarily driven by overall signal

variation rather than temporal variability. Spatially, the SD-controlled correlation cluster more prominently involved parietal and occipital electrodes, suggesting involvement of sensory and association cortex as well. Importantly, the results did depend on our modified entropy estimation method, since the frontal correlation cluster was smaller and non-significant when correlating the bias shift with the shift in conventional MSE (cluster $p = 0.37$)(12)(Figure 4B). Note that we still employed our novel sliding window approach for comparison with the principal mMSE correlation analysis. Controlling for the participants' perceptual ability to detect targets (quantified with SDT sensitivity measure d' (11)) did not affect the relationship (partial $rho = –0.88$, $p < 0.0001$), ruling out a role of perceptual sensitivity. Please see the supplementary text for details on these analyses. Taken together, these results show that neither EEG signal SD, spectral power, nor perceptual sensitivity can account for the observed relationship between entropy and decision bias, highlighting the unique contribution of neural variability to strategic decision bias shifts.

[INSERT FIGURE 4 AROUND HERE]

Finally, improved perceptual sensitivity has been linked to a transient, post-stimulus decrease in neural variability, referred to as variability 'quenching' (14–16). In addition to midfrontal and lateral occipital and temporal enhancement of mMSE modulation (Figure 5A), we also observed such quenching in shorter mMSE timescales after computing the mMSE modulation with respect to the prestimulus baseline (Figure 5B). However, we found liberal–conservative mMSE quenching neither to be correlated with shifts in bias, nor with shifts in d' (see Figure S4 and supplementary text for details). Taken together, these various findings highlight the unique contribution of neural variability to understanding bias shifts in human decision making, over and above overall brain signal variation and oscillatory neural dynamics.

[INSERT FIGURE 5 AROUND HERE]

Discussion

Strategic decision biases allow organisms to adapt their choices to the context in which decisions are made. Frontal cortex has previously been shown to be involved in strategic bias shifts in humans (21–24) and monkeys (25), but its spatiotemporal neural signature has to date remained elusive. Here, we provide first evidence that flexible adjustment of neural variability in frontal regions (but not signal SD or oscillatory brain dynamics) may underlie such strategic shifts in decision bias. The relationship between shifts in bias and neural variability in frontal regions reported here complements our previous findings in the frequency domain that humans can intentionally control prestimulus 8–12 Hz (alpha) oscillatory power in posterior cortex to strategically bias decision making (10). Notably, we previously observed increased oscillatory 2—6 Hz (theta) power in the liberal condition in the same midfrontal electrodes implicated here in the bias-entropy correlation, but this theta power difference was not correlated with the bias shift. This suggests that the cognitive

process implementing the bias shift may be reflected both in low-frequency spectral power and entropy in midfrontal regions, but that only entropy is linked to the magnitude of the decision-maker's bias shift. One possible explanation for such a dissociation is that spectral power exclusively reflects the amplitude of the signal's oscillatory fluctuations while discarding its phase information. Entropy, in contrast, is sensitive both to (variations in) magnitude and phase of signal fluctuations, since more frequent phase resets will result in a more irregular time-domain signal, in turn increasing entropy. Moreover, entropy is agnostic to the shape of the waveforms present in the signal, unlike spectral analysis, which strictly assumes a sinusoidal waveform (26, 27). Entropy thus provides a more unrestricted description of moment-to-moment fluctuations in neural activity that is highly predictive of decision bias shifts in our data.

In contrast with the central idea in this study that neural variability facilitates cognition, previous work has suggested that a temporary stabilization of neural activity after stimulus onset ('quenching') is beneficial for perception (14, 15). Quenching is in line both with the main principle of SDT that noise suppression aids perception (11) and with the notion of attractor dynamics in neural activity that enable the formation of categorical perceptual decisions (28). Although we also observed quenching after baseline-correcting mMSE, we found no evidence for a change-change relationship between quenching and decision bias or perceptual sensitivity. This suggests that in contrast to our finding that rising variability facilitates a strategic bias shift, the degree to which individuals quench is not related to behavior in our data. We note, however, that quenching and rising of neural variability should not be mutually exclusive concepts, but can in principle occur simultaneously if one considers the different timescales in which these phenomena seem to occur: shorter scales (< 40 ms) for quenching and longer scales (> 40 ms) for rising variability. Future studies could further explore how neural variability quenching and rising in different timescales are related to various aspects of decision making, such as perceptual sensitivity, different kinds of bias (29–31), but also confidence and metacognitive processes (32, 33). Finally, individual decision bias has also been linked to the magnitude of transient dilations of the eye's pupil (34, 35), suggesting a link between pupil-linked neuromodulation (36) and neural variability (5). Further investigation of the relationship between neural variability and neuromodulation could prove fruitful to shed light on the mechanisms underlying neural variability.

Our results suggest that dynamic adjustment of neural variability in frontal regions is crucial for adaptive behavior. Based on our findings, we propose that heightened frontal entropy results from a more dynamic, non-deterministic neural regime that enables an individual to be more prepared to process and act upon uncertain, yet task-relevant information. In the current study, variability (entropy) provides a theoretically driven quantification of the neural instantiation of human decision making (8, 9). We argue that quantifying shifts in neural entropy could help elucidate the mechanisms allowing organisms to adapt to their environment and ultimately increase their chances of survival.

Materials and Methods

We report a novel analysis of a previously published dataset involving a target detection task during two different decision bias manipulations (10).

Subjects Sixteen participants (eight females, mean age 24.1 years, ± 1.64) took part in the experiment, either for financial compensation (EUR 10 per hour) or in partial fulfillment of first year psychology course requirements. Each participant completed three experimental sessions on different days, each session lasting ca. 2 hours, including preparation and breaks. One participant completed only two sessions, yielding a total number of sessions across subjects of 47. Due to technical issues, for one session only data for the liberal condition was available. One participant was an author. All participants had normal or corrected-to-normal vision and were right handed. Participants provided written informed consent before the start of the experiment. All procedures were approved by the ethics committee of the University of Amsterdam.

Stimuli Stimuli consisted of a continuous semi-random rapid serial visual presentation (rsvp) of full screen texture patterns. The texture patterns consisted of line elements approx. 0.07° thick and 0.4° long in visual angle. Each texture in the rsvp was presented for 40 ms (i.e. stimulation frequency 25 Hz), and was oriented in one of four possible directions: 0°, 45°, 90° or 135°. Participants were instructed to fixate a red dot in the center of the screen. At random inter trial intervals (ITI's) sampled from a uniform distribution (ITI range 0.3 – 2.2 s), the rsvp contained a fixed sequence of 25 texture patterns, which in total lasted one second. This fixed sequence consisted of four stimuli preceding a (non-)target stimulus (orientations of 45°, 90°, 0°, 90° respectively) and twenty stimuli following the (non)-target (orientations of 0°, 90°, 0°, 90°, 0°, 45°, 0°, 135°, 90°, 45°, 0°, 135°, 0°, 45°, 90°, 45°, 90°, 135°, 0°, 135° respectively) (see Figure 1A). The fifth texture pattern within the sequence (occurring from 0.16 s after sequence onset) was either a target or a nontarget stimulus. Nontargets consisted of either a 45° or a 135° homogenous texture, whereas targets contained a central orientation-defined square of 2.42° visual angle, thereby consisting of both a 45° and a 135° texture. 50% of all targets consisted of a 45° square and 50% of a 135° square. Of all trials, 75% contained a target and 25% a nontarget. Target and nontarget trials were presented in random order. To avoid specific influences on target stimulus visibility due to presentation of similarly or orthogonally oriented texture patterns temporally close in the cascade, no 45° and 135° oriented stimuli were presented directly before or after presentation of the target stimulus. All stimuli had an isoluminance of 72.2 cd/m^2. Stimuli were created using MATLAB (The Mathworks, Inc., Natick, MA, USA) and presented using Presentation version 9.9 (Neurobehavioral systems, Inc., Albany, CA, USA).

Experimental design The participants' task was to detect and actively report targets by pressing a button using their right hand. Targets occasionally went unreported, presumably due to constant forward and backward masking by the continuous cascade of stimuli and unpredictability of target timing (37). The onset of the fixed order of texture patterns preceding and following (non-)target stimuli was neither signaled nor apparent. At the beginning of the experiment, participants were informed they could earn a total bonus of EUR 30, -, on top of their regular pay of EUR 10, - per hour or course credit. In two separate conditions within each session of testing, we encouraged participants to use either a conservative or a liberal bias for reporting targets using both aversive sounds as well as reducing their bonus after errors. In the conservative condition, participants were instructed to only press the button when they were relatively sure they had seen the target. The instruction on

screen before block onset read as follows: 'Try to detect as many targets as possible. Only press when you are relatively sure you just saw a target.' To maximize effectiveness of this instruction, participants were told the bonus would be diminished by 10 cents after a false alarm. During the experiment, a loud aversive sound was played after a false alarm to inform the participant about an error. During the liberal condition, participants were instructed to miss as few targets as possible. The instruction on screen before block onset read as follows: 'Try to detect as many targets as possible. If you sometimes press when there was nothing this is not so bad'. In this condition, the loud aversive sound was played twice in close succession whenever they failed to report a target, and three cents were subsequently deducted from their bonus. The difference in auditory feedback between both conditions was included to inform the participant about the type of error (miss or false alarm), in order to facilitate the desired bias in both conditions. After every block, the participant's score (number of missed targets in the liberal condition and number of false alarms in the conservative condition) was displayed on the screen, as well as the remainder of the bonus. After completing the last session of the experiment, every participant was paid the full bonus as required by the ethical committee.

Participants performed six blocks per session lasting ca. nine minutes each. During a block, participants continuously monitored the screen and were free to respond by button press whenever they thought they saw a target. Each block contained 240 trials, of which 180 target and 60 nontarget trials. The task instruction was presented on the screen before the block started. The condition of the first block of a session was counterbalanced across participants. Prior to EEG recording in the first session, participants performed a 10-min practice run of both conditions, in which visual feedback directly after a miss (liberal condition) or false alarm (conservative) informed participants about their mistake, allowing them to adjust their decision bias accordingly. There were short breaks between blocks, in which participants indicated when they were ready to begin the next block.

Behavioral analysis We defined decision bias as the criterion measure from SDT (11). We calculated the criterion *c* across the trials in each condition as follows:

$$c = -\frac{1}{2}\left[Z(Hit\text{-}rate) + Z(FA\text{-}rate)\right]$$

where hit-rate is the proportion target-present responses of all target-present trials, false alarm (FA)-rate is the proportion target-present responses of all target-absent trials, and Z(...) is the inverse standard normal distribution. Furthermore, we calculated perceptual sensitivity using the SDT measure d`:

$$d' = Z(Hit\text{-}rate) - Z(FA\text{-}rate)$$

EEG recording Continuous EEG data were recorded at 256 Hz using a 48-channel BioSemi Active-Two system (BioSemi, Amsterdam, the Netherlands), connected to a standard EEG cap according to the international 10-20 system. Electrooculography (EOG) was recorded using two electrodes at the outer canthi of the left and right eyes and two electrodes placed above and below the right eye. Horizontal and vertical EOG electrodes were referenced against each other, two for horizontal and two for vertical eye movements (blinks). We used the Fieldtrip toolbox (38) and custom software in MATLAB R2016b (The Mathworks Inc., Natick, MA, USA;

RRID:SCR_001622) to process the data. Data were re-referenced to the average voltage of two electrodes attached to the earlobes. We applied a Butterworth high-pass filter (fourth order, cutoff 0.5 Hz) to remove slow drifts from the data.

Trial extraction We extracted trials of variable duration from 1 s before target sequence onset until 1.25 after button press for trials that included a button press (hits and false alarms), and until 1.25 s after stimulus onset for trials without a button press (misses and correct rejects). The following constraints were used to classify (non-)targets as detected (hits and false alarms), while avoiding the occurrence of button presses in close succession to target reports and button presses occurring outside of trials: 1) A trial was marked as detected if a response occurred within 0.84 s after target onset; 2) when the onset of the next target stimulus sequence started before trial end, the trial was terminated at the next trial's onset; 3) when a button press occurred in the 1.5 s before trial onset, the trial was extracted from 1.5 s after this button press; 4) when a button press occurred between 0.5 s before until 0.2 s after sequence onset, the trial was discarded. After trial extraction the mean of every channel was removed per trial.

Artifact rejection Trials containing muscle artifacts were rejected from further analysis using a standard semi-automatic preprocessing method in Fieldtrip. This procedure consists of bandpass-filtering the trials of a condition block in the 110–125 Hz frequency range, which typically contains most of the muscle artifact activity, followed by a Z-transformation. Trials exceeding a threshold Z-score were removed completely from analysis. We used as the threshold the absolute value of the minimum Z-score within the block, + 1. To remove eye blink artifacts from the time courses, the EEG data from a complete session were transformed using independent component analysis (ICA), and components due to blinks (typically one or two) were removed from the data. In addition, to remove microsaccade-related artifacts we included two virtual channels in the ICA based on channels Fp1 and Fp2, which included transient spike potentials as identified using the saccadic artefact detection algorithm from (Hassler et al., 2011). This yielded a total number of channels submitted to ICA of 48 + 2 = 50. The two components loading high on these virtual electrodes (typically with a frontal topography) were also removed. Blinks and eye movements were then semi-automatically detected from the horizontal and vertical EOG (frequency range 1–15 Hz; z-value cut-off 4 for vertical; 6 for horizontal) and trials containing eye artefacts within 0.1 s around target onset were discarded. This step was done to remove trials in which the target was not seen because the eyes were closed. Finally, trials exceeding a threshold voltage range of 200 mV were discarded. To attenuate volume conduction effects and suppress any remaining microsaccade-related activity, the scalp current density (SCD) was computed using the second-order derivative (the surface Laplacian) of the EEG potential distribution (39).

ERP removal We removed stimulus-evoked EEG activity related to external events by computing the event-related potential (ERP) and subtracting the ERP from each single trial prior to entropy or spectral analysis. This was done to focus on ongoing (termed "induced", (40)) activity and eliminate large-amplitude transients from the data that would increase the signal standard deviation and thus affect the r parameter that is used for determining pattern matches. To eliminate differences in evoked responses between sessions and conditions, we performed this procedure separately for ERPs computed in each condition, session, and participant.

MSE computation We measured temporal neural variability in the EEG using multiscale entropy (MSE) (12). MSE characterizes signal complexity across various time scales by measuring its predictability over time. Typically, MSE relies on the estimation of the sample entropy (SampEn) at each time scale of interest. As succinctly explained in (17), the estimation of SampEn within a given time series involves counting how often patterns of m successive data points reoccur in time (Um) and counting how often patterns of $m + 1$ data points reoccur in time (Um+1). Importantly, given that amplitude values are rarely exactly equal in physiological time series, a similarity parameter is required to define when a data pattern has "reoccurred". A parameter r is set that represents a proportion of the time series standard deviation (SD), thus defining a boundary within which data points are considered equal (see gray horizontal bars in Figure 2A, bottom). This procedure in effect discretizes the data, allowing for comparison of data patterns rather than exact data values. That is, for any data point k, all data points within $k \pm r \times SD$ are by definition equal to k. SampEn is then given as the natural log of $Um(r)/Um+1(r)$. Consequently, high SampEn values indicate low predictability (or higher randomness) of data patterns by indicating that patterns of length $m + 1$ reoccur less often than patterns of length m (i.e., the higher the ratio $Um(r)/Um+1(r)$, the higher SampEn and vice versa). We used parameter settings $m = 2$ and $r = 0.5$, as is typically done in EEG studies involving MSE (41, 42).

Discontinuous MSE computation An important limitation of MSE is the need for substantial continuous data for robust estimation. Heuristically, the recommended number of successive data points for estimation at each scale is 100 (minimum) to 900 (preferred) points using typical MSE parameter settings (Grandy et al., 2016). This limitation precludes the application of MSE to neuroimaging data recorded during cognitive processes that unfold over brief periods of time, such as perceptual decisions. (17) showed that the pattern counting process can be extended to discontinuous data segments that are concatenated across time, as long as the counting of artificial patterns across the segment borders is avoided (as these patterns are a product of the concatenation and do not occur in the data itself). We applied the MSE computation across discontinuous segments of 0.5 s duration (window size). To track the evolution of MSE over the trial, we slid this window across the trials in steps of 50 milliseconds from -0.2 s until 0.6 s, each time recomputing MSE across segments taken from the time window in each trial.

Time series coarsegraining By counting the reoccurrences of patterns of adjacent data points, SampEn measures entropy at the time scale of the signal's sampling rate, which is in the order of milliseconds or shorter in EEG data. To enable estimation of entropy at longer time scales, the time series is typically coarsegrained by averaging groups of adjacent samples ('point averaging') and repeating the entropy computation (12). However, despite its simplicity, this method is suboptimal for eliminating short temporal scales. Point averaging is equivalent to low-pass filtering using a finite-impulse response filter, which does not effectively eliminate higher frequencies and can introduce aliasing (43, 44). For this reason, (44) introduced an improved coarse graining procedure involving replacement of the multi-point average by a low-pass Butterworth filter, which has a well-defined frequency cutoff and precludes aliasing (Figure 6A). The filter cutoff frequency is determined by the ratio of 1 and the scale number, such that an increasingly larger portion of the higher frequencies is removed for slower time scales. Notably, low-pass filtering affects the temporal structure of the time-domain signal, which could

hamper the interpretation of the EEG dynamics due to smearing of responses (45). This issue is largely mitigated, however, due to the liberal–conservative subtraction that we perform before correlating with behavior, since this issue presumably affects both conditions similarly. Filtering is followed by a point-skipping procedure to reduce the signal's sampling rate (Figure 6B). Since point-skipping omits increasingly large portions of the filtered time series depending on the starting point of the point-skipping procedure, we counted patterns separately for each starting point within a scale, summed their counts and computed entropy as described above. Given our segments of 0.5 s window length sampled at 256 Hz, we computed MSE for scales 1 (129 samples within the window) until 42 (three or four samples within the window, depending on the starting point). Note that using a pattern parameter of m = 2, a minimum of three samples within a segment is required to estimate entropy across the segments of continuous data, yielding a maximum possible scale of 42. In line with the MSE literature (46), we converted the time scale units to milliseconds by taking the duration between adjacent data points after each coarsegraining step. For example, time scale 1 corresponds to 1000 ms / 256 Hz = 3.9 ms, and scale 42 to 1000 / (256/42) = 164 ms.

[INSERT FIGURE 6 AROUND HERE]

Pattern similarity parameter computation at each time scale By increasingly smoothing the time series, coarse-graining affects not only on the signal's entropy, but also its overall variation, as reflected in the decreasing standard deviation as a function of time scale (20). In the original implementation of the MSE calculation, the similarity parameter r was set as a proportion of the original (scale 1) time series' standard deviation and applied to all the scales (12). Because of the decreasing variation in the time series due to coarse graining, the similarity parameter therefore becomes increasingly tolerant at slower time scales, resulting in more similar patterns and decreased entropy. This decreasing entropy can be attributed both to changes in signal complexity, but also in overall variation. To overcome this limitation, we recomputed the similarity parameter for each scale, thereby normalizing MSE with respect to changes in overall time series variation at each scale (13).

Spectral analysis We used a sliding window Fourier transform; step size, 50 ms; window size, 500 ms; frequency resolution, 2 Hz) to calculate time-frequency representations (spectrograms) of the EEG power for each electrode and each trial. We used a single Hann taper for the frequency range of 3–35 Hz (spectral smoothing, 4.5 Hz, bin size, 1 Hz) and the multitaper technique for the 36 – 100 Hz frequency range (spectral smoothing, 8 Hz; bin size, 2 Hz; five tapers)(47). See (10) for similar settings. Finally, to investigate spectral power between 1-3 Hz (delta band), we performed an additional time-frequency analysis with a window size of 1 s (i.e. frequency resolution 1 Hz) without spectral smoothing (bin size 0.5 Hz). Spectrograms were aligned to the onset of the stimulus sequence containing the (non)target. Power modulations during the trials were quantified as the percentage of power change at a given time point and frequency bin, relative to a baseline power value for each frequency bin. We used as a baseline the mean EEG power in the interval 0.4 to 0 s before trial onset, computed separately for each condition. If this interval was not completely present in the trial due to preceding events (see Trial

extraction), this period was shortened accordingly. We normalized the data by subtracting the baseline from each time-frequency bin and dividing this difference by the baseline (x 100 %).

Statistical significance testing of EEG power modulations and correlations across space, time and timescale/frequency. To determine clusters of significant modulation with respect to the pre-stimulus baseline without any a priori selection, we ran statistics across space-time-frequency bins using paired t-tests across subjects performed at each bin. Single bins were subsequently thresholded at $p < 0.05$ and clusters of contiguous time-space-frequency bins were determined. For the correlation versions of this analysis, we correlated the brain measure at each bin with the criterion and converted the r-values to a t-statistic using the Fisher-transformation (48). We used a cluster-based procedure (18) to correct for multiple comparisons using a cluster-formation alpha of $p < 0.05$ and a cluster-corrected alpha of $p = 0.05$, two-tailed. For visualization purposes, we integrated (using MATLAB's trapz function) power or entropy values in the time-frequency/entropy representations (TFR/TTR) across the highlighted electrodes in the topographies. For the topographical scalp maps, modulation was integrated across the saturated time-frequency bins in the TFRs/TTRs. See (10) for a similar procedure in the time-frequency domain.

Correlation analysis We used both Pearson correlation and robust Spearman correlation across participants to test the relationships between the behavioral variables as well as with the EEG entropy and power (modulation). To test whether behavior and EEG activity were linked within participants, we used repeated measures correlation. Repeated measures correlation determines the common within-individual association for paired measures assessed on two or more occasions for multiple individuals by controlling for the specific range in which individuals' measurements operate, and correcting the correlation degrees of freedom for non-independence of repeated measurements obtained from each individual (19, 49). To test whether spectral power could account for the observed correlation between criterion and mMSE, we used partial Spearman and Pearson correlation controlling for other variables.

Data and code sharing The data analyzed in this study are publicly available on Figshare (50). We programmed mMSE analysis in a MATLAB function within the format of the FieldTrip toolbox (38). Our ft_entropyanalysis.m function takes data as produced by Fieldtrip's ft_preprocessing.m function as input. In our function, we employed matrix computation of mMSE for increased speed, which is desirable due to the increased computational demand with multi-channel data analyzed with a sliding window. The function supports GPU functionality to further speed up computations. The function is available online (https://github.com/LNDG/mMSE).

Acknowledgments: Funding: Emmy Noether Grant to Douglas D Garrett, Max Planck UCL Centre for Computational Psychiatry and Ageing Research to Douglas Garrett, Niels Kloosterman, and Max Planck Society. **Author contributions:** Niels Kloosterman, Conceptualization, Data curation, Software, Formal analysis, Investigation, Visualization, Methodology, Writing—original draft, Project administration, Writing—review and editing; Julian Kosciessa, Software, Formal analysis, Writing—review and editing; Ulman Lindenberger, Resources, Funding

acquisition, Writing—review and editing; Johannes Jacobus Fahrenfort, Conceptualization, Data curation, Software, Formal analysis, Supervision, Visualization, Methodology, Writing—original draft, Project administration, Writing—review and editing; Douglas Garrett, Conceptualization, Resources, Formal analysis, Supervision, Funding acquisition, Investigation, Methodology, Writing—review and editing. **Competing interests:** Authors declare no competing interests. **Data and materials availability:** All data analyzed during this study are publicly available (50). Analysis scripts are publicly available on Github (https://github.com/nkloost1/critEEGentropy, https://github.com/LNDG/mMSE).

References

1. D. Rahnev, D. Nee, J. Riddle, A. Larson, M. D'Esposito, Causal evidence for frontal cortex organization for perceptual decision making. *Proc National Acad Sci* **113**, 6059–6064 (2016).

2. G. E. Reckless, *et al.*, The left inferior frontal gyrus is involved in adjusting response bias during a perceptual decision making task. *Brain Behav* **4**, 398–407 (2014).

3. M.-Y. Chen, K. Jimura, C. N. White, T. W. Maddox, R. A. Poldrack, Multiple brain networks contribute to the acquisition of bias in perceptual decision-making. *Front Neurosci-switz* **9**, 63 (2015).

4. S. Windmann, T. P. Urbach, M. Kutas, Cognitive and Neural Mechanisms of Decision Biases in Recognition Memory. *Cereb Cortex* **12**, 808–817 (2002).

5. D. D. Garrett, *et al.*, Amphetamine modulates brain signal variability and working memory in younger and older adults. *Proc National Acad Sci* **112**, 7593–7598 (2015).

6. D. D. Garrett, *et al.*, Moment-to-moment brain signal variability: A next frontier in human brain mapping? *Neurosci Biobehav Rev* **37**, 610 624 (2013).

7. D. D. Garrett, N. Kovacevic, A. R. McIntosh, C. L. Grady, The importance of being variable. *J Neurosci* **31**, 4496 4503 (2011).

8. S. E. Marzen, S. DeDeo, The evolution of lossy compression. *J Roy Soc Interface* **14**, 20170166 (2017).

9. W. F. Młynarski, A. M. Hermundstad, Adaptive coding for dynamic sensory inference. *Elife* **7**, e32055 (2018).

10. N. A. Kloosterman, *et al.*, Humans strategically shift decision bias by flexibly adjusting sensory evidence accumulation. *Elife* **8**, e37321 (2019).

11. D. Green, J. Swets, Signal detection theory and psychophysics. *Society* **1**, 521 (1966).

12. M. Costa, A. L. Goldberger, C.-K. Peng, Multiscale entropy analysis of complex physiologic time series. *Phys Rev Lett* **89**, 068102 (2002).

13. J. Q. Kosciessa, N. A. Kloosterman, D. D. Garrett, Standard multiscale entropy reflects spectral power at mismatched temporal scales: What's signal irregularity got to do with it? *Biorxiv*, 752808 (2019).

14. A. Arazi, N. Censor, I. Dinstein, Neural Variability Quenching Predicts Individual Perceptual Abilities. *J Neurosci* **37**, 97 109 (2017).

15. A. Schurger, I. Sarigiannidis, L. Naccache, J. D. Sitt, S. Dehaene, Cortical activity is more stable when sensory stimuli are consciously perceived. *Proc National Acad Sci* **112**, E2083–E2092 (2015).

16. M. M. Churchland, *et al.*, Stimulus onset quenches neural variability: a widespread cortical phenomenon. *Nat Neurosci* **13**, 369 378 (2010).

17. T. H. Grandy, D. D. Garrett, F. Schmiedek, M. Werkle-Bergner, On the estimation of brain signal entropy from sparse neuroimaging data. *Sci Rep-uk* **6**, 23073 (2016).

18. E. Maris, R. Oostenveld, Nonparametric statistical testing of EEG- and MEG-data. *J Neurosci Meth* **164**, 177–190 (2007).

19. J. Z. Bakdash, L. R. Marusich, Repeated Measures Correlation. *Front Psychol* **8**, 491 (2017).

20. V. V. Nikulin, T. Brismar, Comment on "Multiscale entropy analysis of complex physiologic time series". *Phys Rev Lett* **92**, 089803 author reply 089804 (2004).

21. D. Rahnev, D. Nee, J. Riddle, A. Larson, M. D'Esposito, Causal evidence for frontal cortex organization for perceptual decision making. *Proc National Acad Sci* **113**, 6059–6064 (2016).

22. M.-Y. Chen, K. Jimura, C. N. White, T. W. Maddox, R. A. Poldrack, Multiple brain networks contribute to the acquisition of bias in perceptual decision-making. *Front Neurosci-switz* **9**, 63 (2015).

23. S. Windmann, T. P. Urbach, M. Kutas, Cognitive and Neural Mechanisms of Decision Biases in Recognition Memory. *Cereb Cortex* **12**, 808–817 (2002).

24. G. E. Reckless, *et al.*, The left inferior frontal gyrus is involved in adjusting response bias during a perceptual decision□making task. *Brain Behav* **4**, 398–407 (2014).

25. V. P. Ferrera, M. Yanike, C. Cassanello, Frontal eye field neurons signal changes in decision criteria. *Nat Neurosci* **12**, 1458 1462 (2009).

26. S. R. Jones, When brain rhythms aren't 'rhythmic': implication for their mechanisms and meaning. *Curr Opin Neurobiol* **40**, 72–80 (2016).

27. S. R. Cole, B. Voytek, Brain Oscillations and the Importance of Waveform Shape. *Trends Cogn Sci* **21**, 137–149 (2017).

28. X.-J. Wang, Probabilistic Decision Making by Slow Reverberation in Cortical Circuits. *Neuron* **36**, 955–968 (2002).

29. S. M. Fleming, C. L. Thomas, R. J. Dolan, Overcoming status quo bias in the human brain. *Proc National Acad Sci* **107**, 6005–6009 (2010).

30. A. E. Urai, J. de Gee, K. Tsetsos, T. H. Donner, Choice history biases subsequent evidence accumulation. *Elife* **8**, e46331 (2019).

31. B. Talluri, A. E. Urai, K. Tsetsos, M. Usher, T. H. Donner, Confirmation Bias through Selective Overweighting of Choice-Consistent Evidence. *Curr Biol* **28** (2018).

32. N. Yeung, C. Summerfield, Metacognition in human decision-making: confidence and error monitoring. *Philosophical Transactions Royal Soc B Biological Sci* **367**, 1310–1321 (2012).

33. S. M. Fleming, R. J. Dolan, The neural basis of metacognitive ability. *Philosophical Transactions Royal Soc B Biological Sci* **367**, 1338–1349 (2012).

34. J. de Gee, T. Knapen, T. H. Donner, Decision-related pupil dilation reflects upcoming choice and individual bias. *Proc National Acad Sci* **111**, E618 25 (2014).

35. J. de Gee, *et al.*, Dynamic modulation of decision biases by brainstem arousal systems. *Elife* **6**, 309 (2017).

36. S. Joshi, Y. Li, R. M. Kalwani, J. I. Gold, Relationships between Pupil Diameter and Neuronal Activity in the Locus Coeruleus, Colliculi, and Cingulate Cortex. *Neuron* **0**, 221 234 (2015).

37. J. Fahrenfort, H. Scholte, V. Lamme, Masking disrupts reentrant processing in human visual cortex. *Journal of Cognitive Neuroscience* **19**, 1488 1497 (2007).

38. R. Oostenveld, P. Fries, E. Maris, J.-M. Schoffelen, FieldTrip: open source software for advanced analysis of MEG, EEG, and invasive electrophysiological data. *Comput Intel Neurosc* **2011**, 1 9 (2011).

39. F. Perrin, J. Pernier, O. Bertrand, J. Echallier, Spherical splines for scalp potential and current density mapping. *Electroen Clin Neuro* **72**, 184 187 (1989).

40. W. Klimesch, H. Russegger, ppelmayr, T. Pachinger, A method for the calculation of induced band power: implications for the significance of brain oscillations. *Electroencephalogr Clin Neurophysiology Evoked Potentials Sect* **108**, 123 130 (1998).

41. J. S. Richman, R. J. Moorman, Physiological time-series analysis using

approximate entropy and sample entropy. *Phys Rev A* **278**, H2039 H2049 (2000).

42. J. J. Heisz, A. R. McIntosh, Applications of EEG Neuroimaging Data: Event-related Potentials, Spectral Power, and Multiscale Entropy. *J Vis Exp Jove*, 50131 (2013).

43. J. Semmlow, Signal Processing and Communications. **22** (2004).

44. J. Valencia, *et al.*, Refined multiscale entropy: application to 24-h Holter recordings of heart period variability in healthy and aortic stenosis subjects. *Ieee T Bio-med Eng* **56**, 2202 2213 (2009).

45. R. VanRullen, Four Common Conceptual Fallacies in Mapping the Time Course of Recognition. *Front Psychol* **2**, 365 (2011).

46. J. Courtiol, *et al.*, The multiscale entropy: Guidelines for use and interpretation in brain signal analysis. *J Neurosci Meth* **273**, 175 190 (2016).

47. P. Mitra, H. Bokil, Observed Brain Dynamics - Partha Mitra, Hemant Bokil - Google Books (2007).

48. R. Fisher, Frequency Distribution of the Values of the Correlation Coefficient in Samples from an Indefinitely Large Population. *Biometrika* **10**, 507 (1915).

49. M. J. Bland, D. G. Altman, Statistics notes: Calculating correlation coefficients with repeated observations: Part 1—correlation within subjects. *Bmj* **310**, 446 446 (1995).

50. N. A. Kloosterman, *et al.*, Data from: Humans strategically shift decision bias by flexibly adjusting sensory evidence accumulation in visual cortex (2018) https:/doi.org/https://doi.org/10.6084/m9.figshare.6142940 .

Figures and Tables

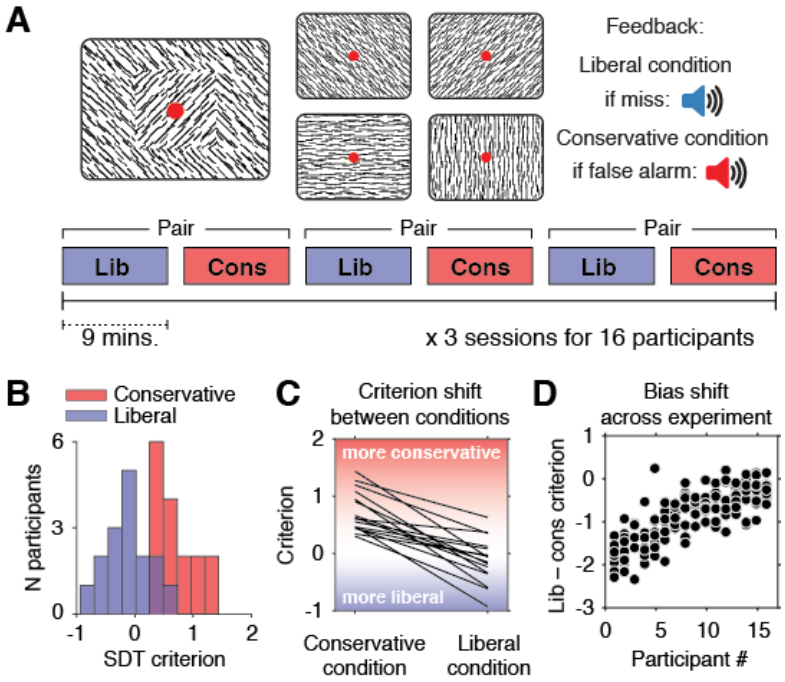

Figure 1 | **Experimental paradigm and behavioral results A.** Top, target and non-target stimuli. Subjects detected targets (left panel) within a continuous stream of diagonal and cardinal line stimuli (middle panel), and reported targets via a button press. In different blocks of trials, subjects were instructed to actively avoid either target misses (liberal condition) or false alarms (conservative condition). Auditory feedback was played directly after the respective error in both conditions (right panel). Bottom, time course of an experimental session. The two conditions were alternatingly administered in blocks of nine minutes. In between blocks participants were informed about current task performance and received instructions for the next block. Subsequent liberal and conservative blocks were paired for within-participant analyses (see panel D, and Figure 3C). **B.** Distributions of participants' criterion in both conditions. A positive criterion indicates a more conservative bias, whereas a negative criterion indicates a more liberal bias. **C.** Corresponding within-person slopes. **D.** Within-person bias shifts for liberal–conservative block pairs (see panel A, bottom). Participants were sorted based on average criterion shift before plotting. Please see Figure S1 for the results on perceptual sensitivity.

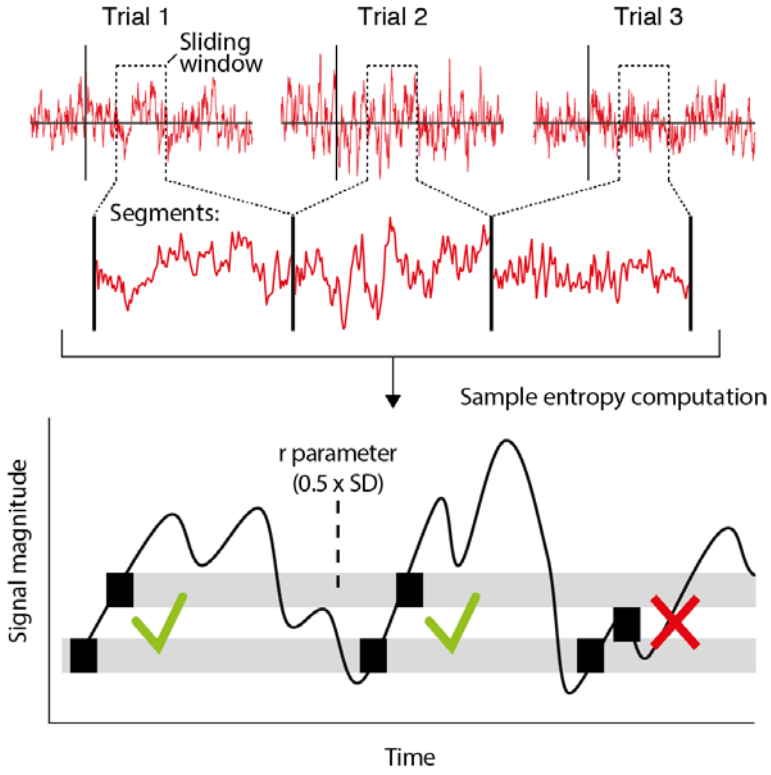

Figure 2 | mMSE estimation procedure. Discontinuous entropy computation procedure. Top row, data segments of 0.5 s duration centered on a specific time point from each trial's onset are concatenated (middle row). Bottom, entropy is then computed on this concatenated time series while excluding discontinuous segment borders by counting repeats of both m (here, 2) and m+1 sample patterns and taking the log ratio of the two pattern counts. The pattern similarity parameter r determines whether or not a pattern is counted as a repeat, indicated by the horizontal gray bars. The procedure is repeated at each step of the sliding window, resulting in a time course of entropy estimates computed across trials.

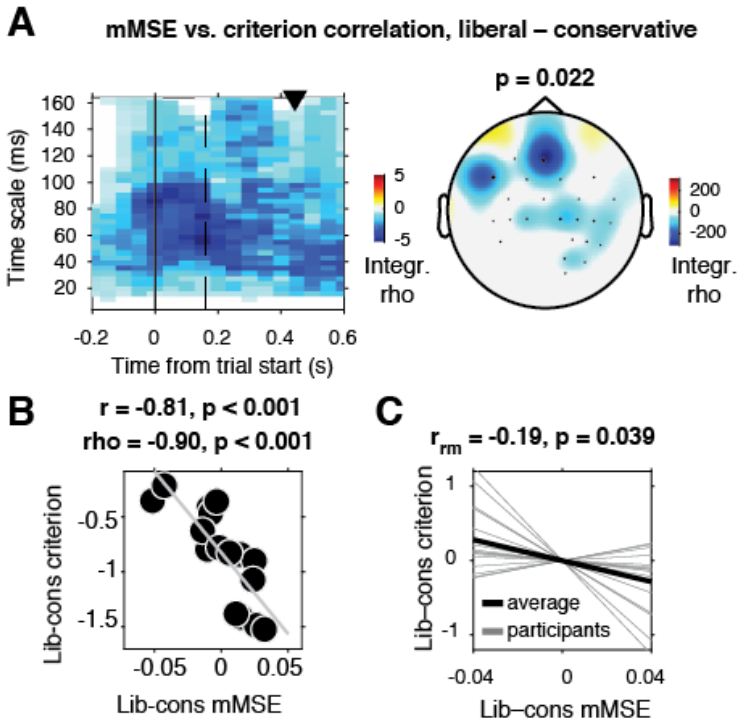

Figure 3 | Change-change correlation between Liberal–conservative mMSE vs. bias shift. A. Significant negative electrode-time-timescale cluster observed via Spearman correlation between liberal–conservative mMSE and liberal–conservative SDT criterion. Correlations outside the significant cluster are masked out. Left, time-timescale representation showing the correlation cluster integrated over the electrodes indicated by the black circles in the topographical scalp map. The solid vertical line indicates the time of trial onset. The dotted vertical line indicates time of (non)target onset. Right, scalp map of mMSE integrated across significant time-timescale bins. P-value above scalp map indicates multiple comparison-corrected cluster significance using a permutation test across participants. **B.** Scatter plot of the correlation after averaging mMSE within the significant cluster. Both Pearson's r and Spearman's rho are indicated. **C.** Single-subject mMSE vs. criterion slopes across liberal–conservative block pairs. r_{rm}, repeated measures correlation across all block pairs performed after centering each subject's shifts in mMSE and criterion around zero.

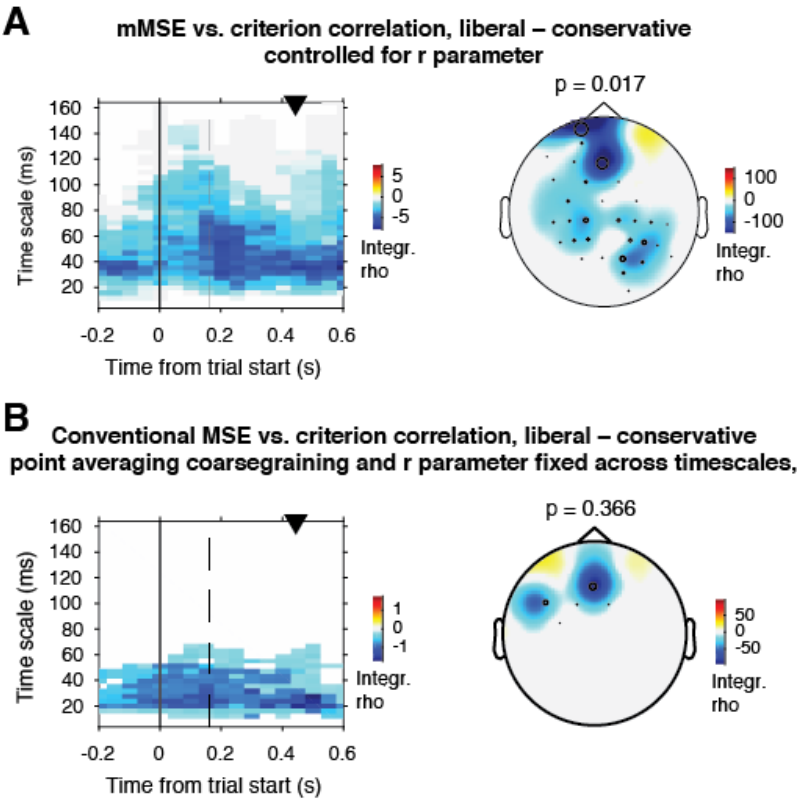

Figure 4 | A. Liberal – conservative mMSE vs. criterion correlation when statistically controlling for the r parameter (signal SD) across participants. The cluster remains significant and the topography is similar, but the effect is more widespread across electrodes, and less widespread across timescales. **B.** As A. but using traditional MSE, including point averaging coarse graining and a fixed r parameter across timescales. The cluster does not reach significance.

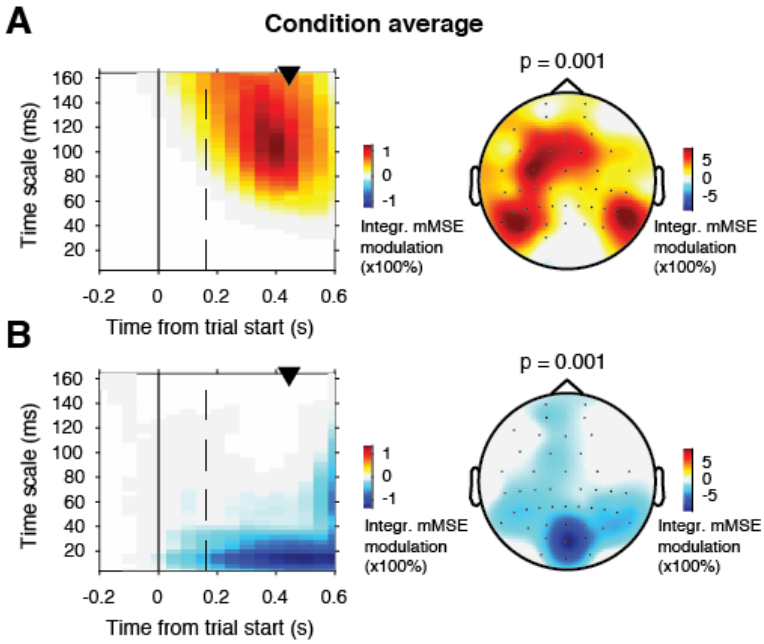

Figure 5 | mMSE modulation with respect to pre-trial baseline. A. Significant positive cluster observed in longer timescales after normalizing mMSE values to percent signal change (%) units with respect to the pre-trial baseline (–0.2 to 0 s) and averaging across conditions. **B.** Negative ("quenching") cluster observed in shorter timescales in posterior electrodes. Conventions as in Figure 3. Please see Figure S5 for relationships with behavior and spectral power modulation.

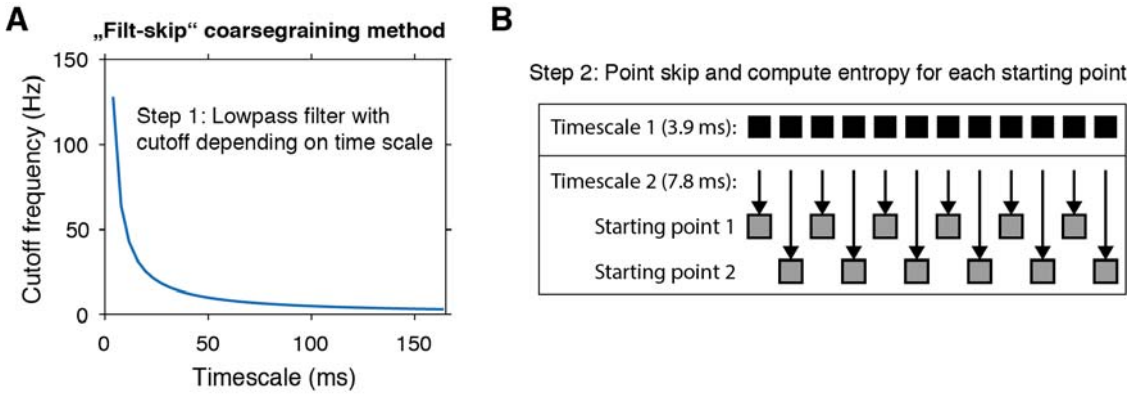

Figure 6 | “Filt-skip” coarsegraining procedure used to estimate entropy on longer timescales. **A.** The method consists of low-pass filtering followed by point-skipping (13). Filter cutoff frequency is determined by dividing the data sampling rate (here, 256 Hz) by the index of the timescale of interest (17). **B.** The signal is then coarsened by intermittently skipping samples. In this example, at timescale 2 every second sample is skipped, resulting in two different time courses depending on starting points. Patterns are counted independently in both time courses and summed before computing entropy.